Tellus
SERIES B
CHEMICAL
AND PHYSICAL
METEOROLOGY
PUBLISHED BY THE INTERNATIONAL METEOROLOGICAL INSTITUTE IN STOCKHOLM

Tellus (2009), 61B, 718–731
Printed in Singapore. All rights reserved

TELLUS

Climate effects on atmospheric carbon dioxide over the last century

By LAUREN ELMEGREEN RAFELSKI*, STEPHEN C. PIPER and RALPH F. KEELING,
Scripps Institution of Oceanography, University of California, San Diego, La Jolla, CA 92093-0244, USA

(Manuscript received 21 November 2008; in final form 21 July 2009)

ABSTRACT

The buildup of atmospheric CO_2 since 1958 is surprisingly well explained by the simple premise that 57% of the industrial emissions (fossil fuel burning and cement manufacture) has remained airborne. This premise accounts well for the rise both before and after 1980 despite a decrease in the growth rate of fossil fuel CO_2 emissions, which occurred at that time, and by itself should have caused the airborne fraction to decrease. In contrast, the buildup prior to 1958 was not simply proportional to cumulative fossil fuel emissions, and notably included a period during the 1940s when CO_2 growth stalled despite continued fossil fuel emissions. Here we show that the constancy of the airborne fraction since 1958 can be in part explained by decadal variations in global land air temperature, which caused a warming-induced release of CO_2 from the land biosphere to the atmosphere. We also show that the 1940s plateau may be related to these decadal temperature variations. Furthermore, we show that there is a close connection between the phenomenology producing CO_2 variability on multidecadal and El Niño timescales.

1. Introduction

Records from the Scripps Institution of Oceanography indicate that the global average CO_2 concentration (based on an average of Mauna Loa and the South Pole) increased from 315 ppm in 1958 to 383 ppm in 2008. Over this period, the airborne fraction computed as a ratio of CO_2 buildup to industrial emissions (fossil fuel plus cement, which we will refer to as 'fossil fuel' emissions) amounts to 57%. In Fig. 1, we show the atmospheric CO_2 record against the cumulative fossil fuel emissions scaled to 57%, following Keeling et al. (1995). Also following Keeling et al. (1995), we detrend the record using this constant airborne fraction (Fig. 1B) to produce an anomaly that we refer to as the constant airborne fraction (CAF) anomaly. From 1958 to the present, the CAF anomaly remains very small, never exceeding 2 ppm, although larger anomalies were present earlier. Similarly, the 2007 IPCC report (Denman et al., 2007) shows that since 1958, the airborne fraction has remained highly constant when averaged for periods of 5 yr or more.

The virtual constancy of the airborne fraction since 1958 requires that the sum of the global carbon sinks and any additional sources (such as CO_2 release from land use) has increased in proportion to fossil fuel emissions. Two major sink processes are expected to respond directly to rising CO_2: ocean CO_2 uptake and CO_2 fertilization of plant growth (DeLucia et al., 1999). However, even if these were the only sink processes, one would expect a constant airborne fraction only if fossil fuel emissions grow at a constant rate per year (Bacastow and Keeling, 1979; Oeschger and Heimann, 1983). In 1980, the growth rate of fossil fuel emissions decreased from ~4.3 to ~1.5% per year, as shown in Fig. 2. This decrease should have caused the airborne fraction to decrease, because carbon sinks are less limited by kinetic barriers when atmospheric CO_2 is rising more slowly. Keeling et al. (1995) suggested that the constancy of the airborne fraction before and after 1980 might result from carbon exchanges driven by climate changes, noting similarities between decadal variations in carbon dioxide and decadal anomalies in global temperature. Carbon sink modelling studies (Dai and Fung, 1993; Houghton, 1995; Cramer et al., 2001) also suggest a link between climate change and carbon exchange, showing that CO_2 releases are associated with periods of warming.

On short timescales, the growth rate of atmospheric CO_2 is far more variable than fossil fuel emissions, reflecting large exchanges of carbon from the land biosphere associated with El Niño events and other short term climate forcing (Keeling et al., 1995). Recent work implicates biomass burning as a potentially large source of this variability (Langenfelds et al., 2002; van der Werf et al., 2004; Randerson et al., 2005). It is unclear if the climate processes involved in this shorter-term variability are also relevant on longer timescales.

Prior to 1958, the growth rate of CO_2 was less closely tied to fossil fuel emissions. Figure 1 shows the most detailed available

*Corresponding author.
e-mail: lelmegre@ucsd.edu
DOI: 10.1111/j.1600-0889.2009.00439.x

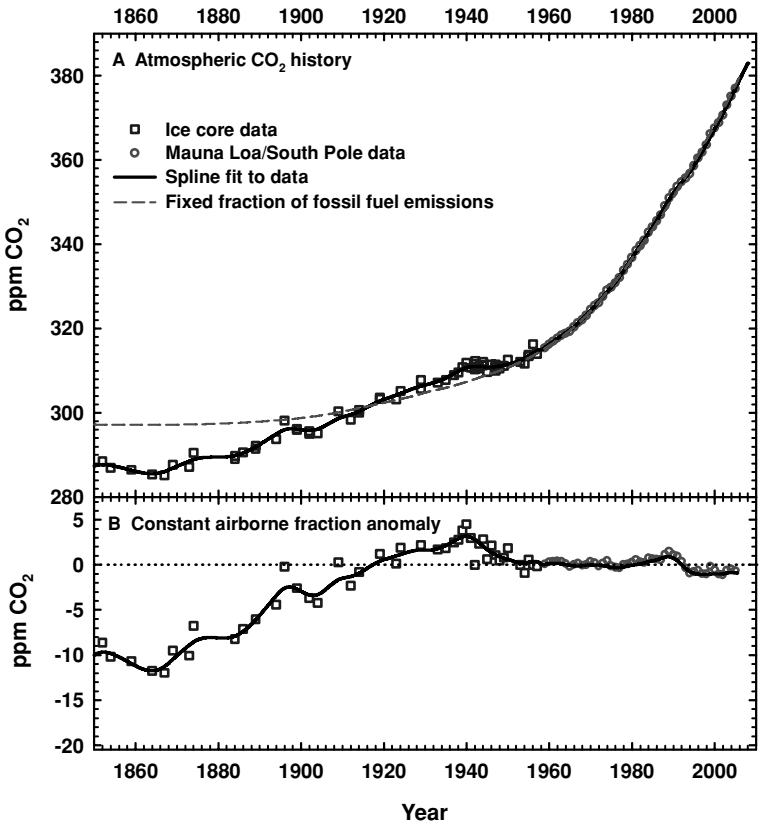

Fig. 1. (A) Atmospheric CO_2 record based on ice core data before 1958, (Etheridge et al., 1996; MacFarling Meure et al., 2006) and yearly averages of direct observations from Mauna Loa and the South Pole after 1958 (from the Scripps CO_2 program). Also shown is a spline fit to the record and a curve depicting 57% of cumulative industrial (fossil fuel and cement) emissions (Marland et al., 2006). (B) Constant airborne fraction anomaly, computed by taking the difference between the atmospheric record and 57% of fossil fuel emissions.

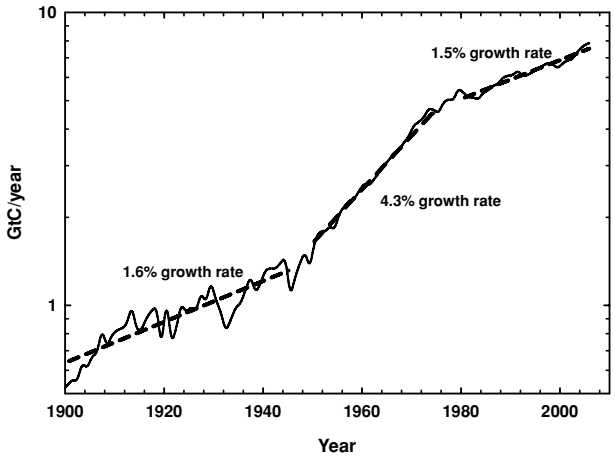

Fig. 2. Fossil fuel emissions per year, plotted on a log scale. The approximate growth rates in fossil fuel emissions from 1900 to 1950, 1950 to 1980 and 1980–present are also plotted.

ice core CO_2 record, from Law Dome, Antarctica (Etheridge et al., 1996; MacFarling Meure et al., 2006), which we use to extend the atmospheric record back to 1850. As is well known, atmospheric CO_2 rose from 1850 to 1900 at a faster rate than expected from fossil fuel emissions (Fig. 1A). During this time period, CO_2 was rising in response to another CO_2 source, most likely emissions from land use changes (Pearman et al., 1986; Siegenthaler and Oeschger, 1987). During the 1940s, the CO_2 buildup stalled in spite of fossil fuel emissions that were at least as high as in previous years.

The near constancy of the airborne fraction since 1958 is all the more striking when compared to these large earlier fluctuations. Until these contrasting behaviours can be understood, it may be difficult to develop reliable forecasts of future variations in the airborne fraction, and hence future atmospheric CO_2 loading. A particular concern is that warming may trigger additional carbon releases, which may amplify global warming in a positive feedback loop (Cox et al., 2000).

Here we explore the carbon sinks since 1850 using the atmospheric mass balance:

$$\Delta CO_2 = F + LU - O - B, \quad (1)$$

where F is fossil fuel emissions, LU is land use CO_2 emissions, O is the ocean sink, and B is the residual land flux. We solve eq. (1) for the time-varying term B, using specified time variations in the other terms, in a calculation known as a 'single deconvolution.' The residual land exchange calculated this way includes the contributions from all land processes other than land use, and from errors in the F, LU and O terms. We compare estimates of this residual land exchange with calculations from a two-box biospheric model, to assess the potential for any unexpected

trends. Following Keeling et al. (1995) this approach emphasizes the need for the inclusion of processes that are tied to changes in global climate on decadal timescales.

2. Methods

2.1. Description of data

We use the fossil fuel emissions record from Marland et al. (2006), which includes yearly values from 1751 to 2003. CO_2 emissions from cement manufacturing are included in these values. Emissions are extrapolated to 2006 using data from the BP Statistical Review of World Energy (BP, 2008), and are linearly interpolated to monthly resolution.

We use estimates of land use CO_2 emissions from 1850 to 2000 from Houghton (2003). The emissions are extrapolated to 2006 by assuming that yearly emissions stayed constant after the year 2000. Land use emission estimates are uncertain to the 50% level (Houghton, 2003), with the highest uncertainties in tropical regions (House et al., 2003; Jain and Yang, 2005). Satellite studies suggest that the Food and Agriculture Organization's (FAO) records of land use change, used by Houghton, may have overestimated the amount of deforestation in the tropics, thereby overestimating tropical emissions (Achard et al., 2002; DeFries et al., 2002). We therefore regard the estimates of Houghton as an upper bound on land use emissions ('high land use emissions' case). To allow for uncertainty in land use, we also consider a low land use emissions case in which, for simplicity, we set the tropical emissions to zero while adopting the extratropical emissions from Houghton. We regard this low land use case as an extreme lower bound. This low land use case is also more similar in shape to land use fluxes modelled by terrestrial biosphere models (McGuire et al., 2001). For the low land use case, emissions were nearly zero at the year 2000. In this case, the global land use flux was assumed to be zero after the year 2000. Fluxes for both cases were linearly interpolated to monthly resolution.

We use a global CO_2 record based on a combination of the ice core record from Law Dome before 1958 (Etheridge et al., 1996; MacFarling Meure et al., 2006) and a seasonally detrended arithmetic average of monthly air measurements from Mauna Loa and the South Pole from the Scripps CO_2 program after 1958 (Fig. 1). The records were combined without adjustment. The ice core data are approximated to monthly resolution using a spline with a standard error, σ, of 0.6 ppm CO_2.

2.2. Ocean model

To represent the oceanic uptake of CO_2, we use a rescaled version of the mixed-layer pulse response function based on the HILDA model, from Joos et al. (1996). We ran the pulse response function model starting at the year 1800 using a one-month time step, and integrated the yearly uptake values to determine the net uptake since 1800. We rescaled the results by multiplying by a constant to achieve 118 PgC for the integrated uptake from 1800 to 1994, consistent with Sabine et al. (2004). Sabine's results are in good agreement with uptake estimates based on the observed trends in atmospheric O_2 concentration (Manning and Keeling, 2006).

In fact, Joos et al. developed pulse response functions not just for the HILDA model, but also for three additional models: a box diffusion model, a 2-D ocean general circulation model (OGCM), and the Princeton 3-D OGCM. We found, however, that the differences between these models were very small once they were rescaled to achieve the same integrated uptake from 1800 to 1994: the yearly oceanic uptakes differed by at most 0.07 PgC yr^{-1}, and the integrated ocean uptake through 2005 differed by at most 0.5 PgC, with the biggest difference occurring between the 3-D model and the other models around 1960.

To allow for uncertainty in oceanic uptake of CO_2, we consider several alternate cases. First, we allow for uncertainty in the Sabine constraint by scaling the ocean uptake uniformly by ±30% ('high ocean uptake' or 'low ocean uptake'). Second, we allow for possible climate effects on ocean uptake by allowing for changes in sea surface temperature (SST) on equilibrium carbon chemistry. We modify the pulse response formulation of Joos et al. so that pCO_2 is computed from the full DIC concentration, not just the perturbation since preindustrial times. This is necessary because changes in SST affect all of the carbon in the mixed layer, not just the perturbation. We use a global SST record since 1850 (Brohan et al., 2006) to drive the ocean model.

This model does not consider the effects of climate change on ocean biology or circulation. However, more complex ocean models suggest that their effects are small globally (Le Quéré et al., 2007) or would lead to uptake intermediate to the cases we consider (Plattner et al., 2001).

2.3. Land model

As a simple depiction of the land biosphere, we use a two-box model. The model uses a 1477 PgC box with a 60 yr turnover time and a 110 PgC box with a 2.5 yr turnover time, as shown in

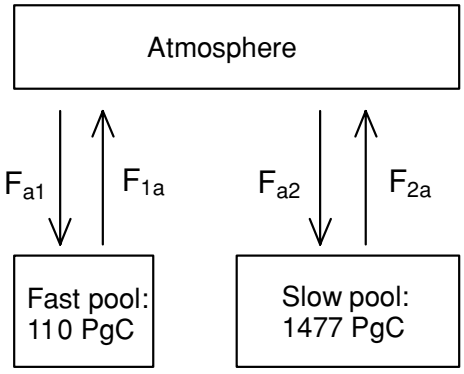

Fig. 3. Terrestrial two-box model.

Fig. 3. The turnover times are consistent with the turnover times of a two-box model used by Bacastow and Keeling (1973). The large box size is from the one-box model used by Keeling et al. (1989), and the small box size is from the 'short lived biota' box of a more complex model presented by Bolin (1986). The total size of our land box differs from that presented in the 2007 IPCC report (Denman et al., 2007). However, as explained below, although the turnover times are important in determining the magnitude of the fluxes, the box sizes are less important, as they are redundant with other parameters once the model is fit to observations.

Prior studies using box models have typically used CO_2 fertilization to drive the land uptake (Keeling et al., 1989). However, recent work suggests that nitrogen fertilization could be equally or more important (Magnani et al., 2007). Here, we allow for both CO_2 and N fertilization as well as the effects of temperature-dependent respiration. These processes are represented according to:

$$F_{ai} = K_{ai} \times C^o_{atm} \times \left(1 + \varepsilon \Delta C_{atm}/C^o_{atm} + \gamma\, ff\right) \quad (2)$$

$$F_{ia} = K_{ia} \times (Q_{10})_i^{(T-T_o)/10} \times (C^o_i + \Delta C_i), \quad (3)$$

where F_{ai} (PgC yr^{-1}) is the allocation from net primary production (NPP) to box i (where $i = 1$ or 2) and F_{ia} is the carbon released by heterotrophic respiration or fire from box i to the atmosphere. K_{ai} and K_{ia} (yr^{-1}) are exchange constants (1/turnover time), ΔC_i (PgC) is the change in box i size since 1850, ε is the fertilization factor from increased CO_2 in the atmosphere, γ ((PgC yr^{-1})$^{-1}$) is the fertilization factor from increased nitrogen, ff (PgC yr^{-1}) is fossil fuel emissions, C° is the initial box size (PgC), and Q_{10} is the factor that the fluxes change for a 10°C temperature change. A global land air temperature record (Brohan et al., 2006) is used to drive the model. The parametrization of N fertilization in Equation (2) is based on Townsend et al. (1996), which allows for excess N from fossil fuel combustion. The parametrization implicitly accounts for N fertilization from other anthropogenic sources that have grown over time in proportion to fossil fuel burning. As in Townsend et al., we ignore the potentially large contribution of industrial nitrogen (Galloway and Cowling, 2002) because this nitrogen is mostly applied to agricultural areas, which do not have long-term carbon storage. Equations (2) and (3) are generalized expressions for the fluxes. We also consider simpler cases in which one or more processes are neglected, for example, by setting $\varepsilon = 0$, $\gamma = 0$ or $Q_{10} = 1$.

Previous studies, such as Jones and Cox (2005), have used statistical regressions with time-series such as the Niño3 index to explore variability in atmospheric CO_2. The two-box model that we use is a more mechanistic approach to understanding variability, allowing for time constants in the response of CO_2 fluxes to forcings. The parameters ε, γ, and Q_{10} are fitted empirically using observed atmospheric CO_2 and carbon emissions records. We find that if we change the box sizes while keeping the time constants the same (not shown), the values of the fitted parameters ε, γ or Q_{10} change, but the carbon flux over time does not change. For this reason, the chosen box sizes are less important than the turnover times, and the magnitude of fitted parameters do not necessarily have simple physiological significance.

3. Results

3.1. Residual flux from deconvolution

A standard case for the residual land exchange from the deconvolution (B in eq. 1) is shown in Fig. 4A (green curve), along with associated land use emissions. This standard case uses constant sea surface temperature (SST), high land use emissions, and a central estimate of oceanic CO_2 uptake (CHM – see Table 1). The residual flux has been smoothed using a 10-year running mean, to reduce the El Niño scale variability. The residual flux estimate in Fig. 4A is similar to previous estimates from 1900 on (Houghton, 2007), with differences in the magnitude of the variability before 1900. Our residual flux oscillates around zero until 1920, after which it increases over time with some notable multidecadal variability. The magnitude of the residual flux is directly tied to the land use emissions. The low land use emissions case (CLM), as shown in Fig. 4B, yields a residual flux which stays much closer to zero than the high land use emissions case, but the pattern of multidecadal variability is largely unchanged.

3.2. Temperature-independent model

We now compare estimates of the residual flux to results from a simple land biosphere model, which consists of the biospheric model driven only by CO_2 fertilization ($\gamma = 0$ and $Q_{10} = 1$). Although here we show results where both boxes respond to fertilization (with the same ε for both boxes), we find that the quality of our fit does not change if only the large box responds to fertilization (results not shown). Both the model output and the residual flux are filtered using a 10-year running mean. A non-linear least-squares regression analysis is used to find the value of ε that best fits the filtered residual flux over the period from 1900 to 2005. Although the model (Figs. 4A and 4B, black curves) reproduces the long-term uptake of the residual, it does not match the decadal variability. The model and deconvolution-based residual curves cross each other around 1940 and 1980, with the modelled sink too large before 1940 and after 1980, and too small between 1940 and 1980.

The decadal pattern is also revealed in the time integrated difference between the deconvolution and model shown in Fig. 4C, which can be expressed as a carbon anomaly in PgC (not to be confused with the CAF anomaly). Because time integration is already a form of low-pass filtering, we compute these anomalies with the 10-year smoothing of the land model output and residual flux removed. For both the high and low land use

cases, the anomaly curves have a similar overall shape, with the anomaly rising until 1940, falling until 1976, and then remaining relatively constant (CHM-C) or rising slightly (CLM-C).

The shape of the CO_2 anomaly curves in Fig. 4C have an obvious similarity to the shape of the global land air temperature record (Brohan et al., 2006) shown in Fig. 4D, which also has breaks in slope around 1940 and 1976. This similarity supports

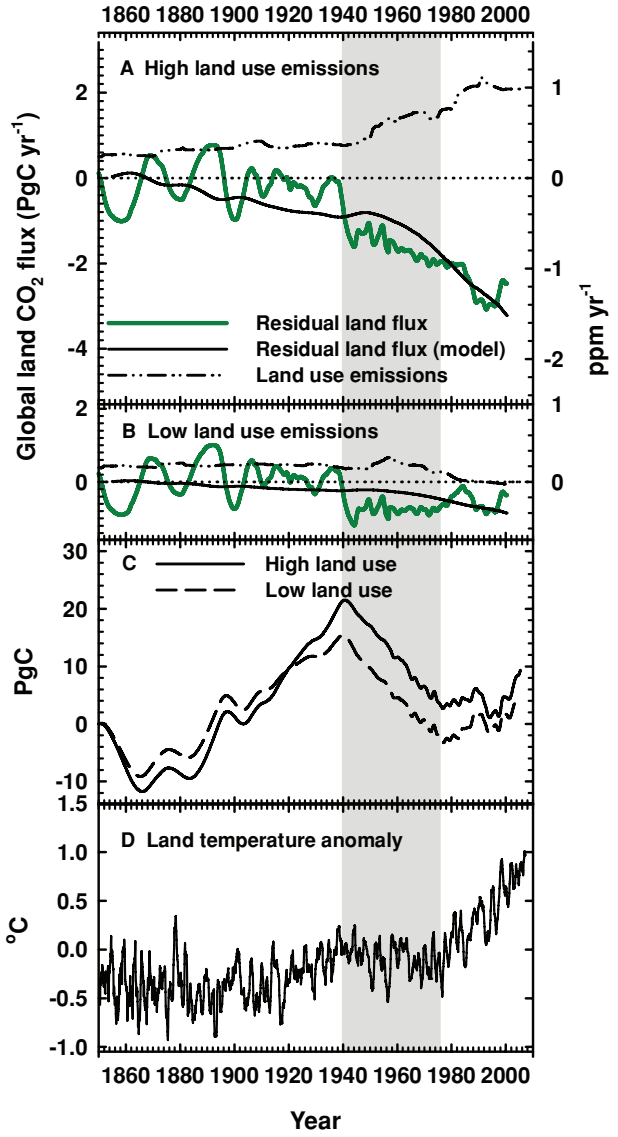

Fig. 4. Residual land carbon fluxes based on a deconvolution and based on the temperature-independent model. Sources to the atmosphere are plotted as positive, and sinks are plotted as negative. (A) The high land use emissions case (CHM-C) and (B) the low land use emissions case (CLM-C). (C) The integrated difference between the model and residual land fluxes. (D) Global land air temperature anomaly relative to the 1961–1990 mean (Brohan et al., 2006). Grey area highlights the period of relatively constant or decreasing global land air temperature from 1940 to 1976.

Table 1. (A) Parameters used for calculations of the residual land flux

Case	Description		
	SST	Land Use	Ocean Uptake
CHM	Constant	High	Medium
CLM	Constant	Low	Medium
CHL	Constant	High	Low
CHH	Constant	High	High
CLL	Constant	Low	Low
CLH	Constant	Low	High
VHM	Variable	High	Medium
VLM	Variable	Low	Medium

B) Model Parameters

Parameters	Description	
	Fertilization method	Q_{10}
-C	CO_2 only	Defined as 1
-V	CO_2 only	Fit to land air temperature record
-CN	Nitrogen only	Defined as 1
-VN	Nitrogen only	Fit to land air temperature record

the findings (Dai and Fung, 1993; Houghton, 1995; Keeling et al., 1995; Cramer et al., 2001) that processes tied to temperature may be responsible for the pattern of multidecadal CO_2 fluxes not accounted for in the model.

As a third way of looking at the CO_2 anomaly of our model, we add the fluxes from fossil fuel emissions, land use change emissions, and ocean uptake to our modelled land uptake (as in eq. 1), and integrate the net flux over time, adding an integration constant to achieve the best agreement with the CO_2 record from 1959 to 1979 (shown for CHM-C in Fig. 5). We again use a modelled land uptake with the 10-yr smoothing removed. To better display small trend differences, we detrend the modelled CO_2 concentration using 57% of fossil fuel emissions, as in Fig. 1B. Looking at the slopes of the lines in Fig. 5, the modelled CO_2 is seen to rise too slowly from 1880 to 1940, too rapidly from 1940 to 1980, and too slowly from 1980 to the present compared to observations. The difficulty in matching the constancy in the airborne fraction before and after 1980 in this class of model was noted previously by Keeling et al. (1995).

3.3. *Temperature-dependent model*

We now repeat the same analysis, allowing for temperature-dependent respiration (relaxing the requirement that $Q_{10} = 1$) driven by changes in the global land air temperature record. We thus now fit both ε and Q_{10}. We find (results not shown) that allowing temperature-dependent respiration in the large land box does not affect the fit. Because of the 60-yr time constant of this box, the Q_{10} parameter only influences the long-term flux, which is already optimized by fitting ε. To avoid such redundancy in

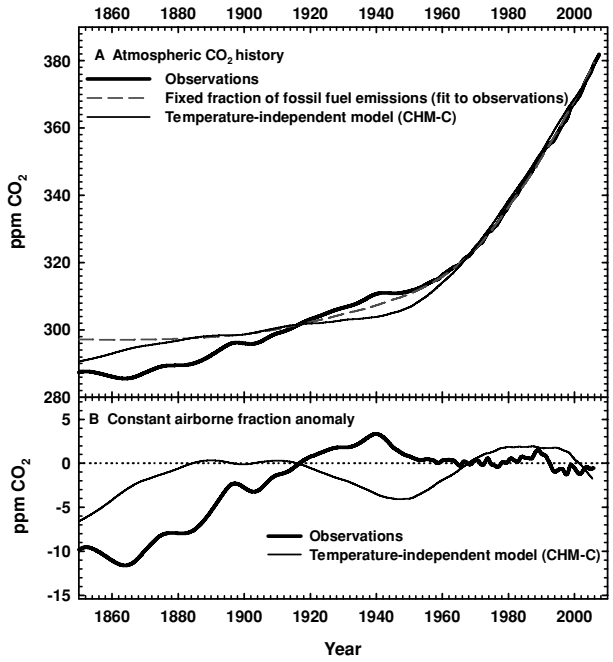

Fig. 5. (A) Atmospheric CO_2 record, atmospheric CO_2 modelled using the temperature-independent model, and a curve depicting 57% of cumulative industrial (fossil fuel and cement) emissions. An integration constant has been added to the modelled atmospheric CO_2 to match observations from 1959 to 1979. (B) Constant airborne fraction anomaly of the atmospheric record and model results, computed by taking the difference between the atmospheric record and 57% of fossil fuel emissions.

the fit, we therefore only allow temperature-dependence in the small box, thus setting $Q_{10} = 1$ for the large box, and optimally fitting Q_{10} for the small box. The parameter ε is again fit for both boxes. This two-parameter fit tracks the multidecadal variability more closely (Fig. 6). When the fossil fuel, land use, and ocean carbon fluxes are added to the modelled residual land flux and integrated over time, we find that the temperature-dependent model does a better job than the temperature-independent model of reproducing the atmospheric CO_2 record from 1920-present (shown for CHM-V in Fig. 7). In particular, the model now does a better job of reproducing the low growth from 1940 to 1950, and matching the accelerating growth from 1960 to 1980 and from 1980 to the present. In other words, the model does a better job of reproducing the 1940s plateau and the overall constancy of the airborne fraction since 1960. Even with the improved fit, however, the model does not perfectly track the multidecadal variability: the model underestimates the overall CO_2 rise before 1940, predicts a rise that is too rapid in the late 1950s, and overpredicts atmospheric CO_2 concentrations from around 1991 to 2002. These features are discussed further below.

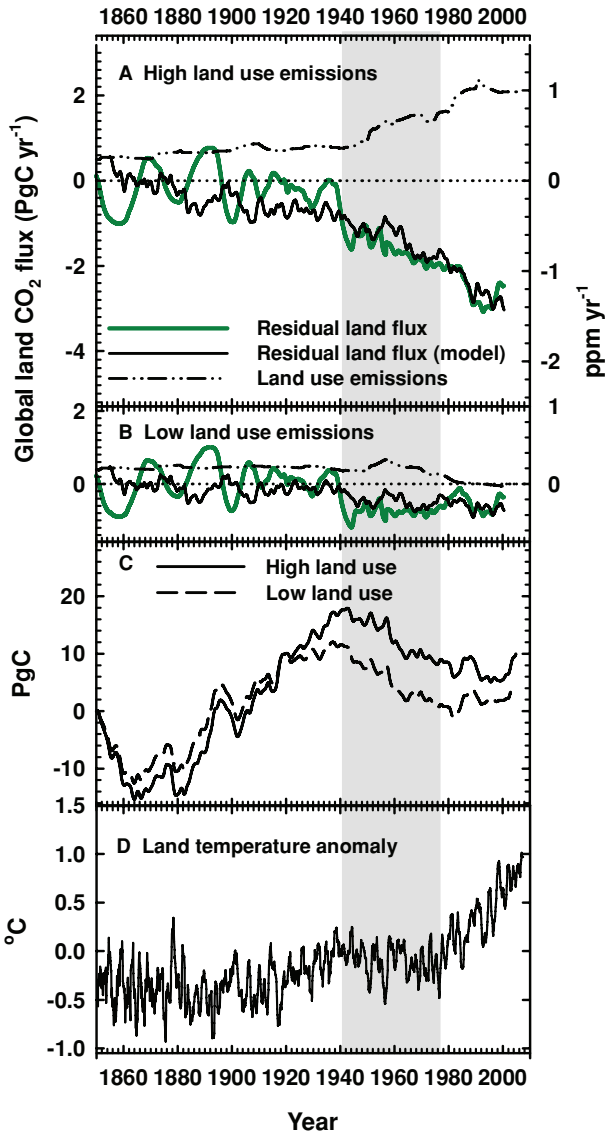

Fig. 6. Residual land carbon fluxes based on a deconvolution and based on the temperature-dependent model. Sources to the atmosphere are plotted as positive, and sinks are plotted as negative. (A) The high land use emissions case (CHM-V) and (B) the low land use emissions case (CLM-V). (C) The integrated difference between the model and residual land fluxes. (D) Global land air temperature anomaly relative to the 1961–1990 mean (Brohan et al., 2006). Grey area highlights the period of relatively constant or decreasing global land air temperature from 1940 to 1976.

3.4. *Sensitivity analyses*

The analysis in the previous section is subject to uncertainties in the residual land flux that remain to be addressed. The analysis explored uncertainty in land use emissions, but not in ocean uptake, nor did it consider the possibility of nitrogen fertilization.

To address these and other uncertainties, we consider a matrix of different cases, as detailed in Table 2. For these cases,

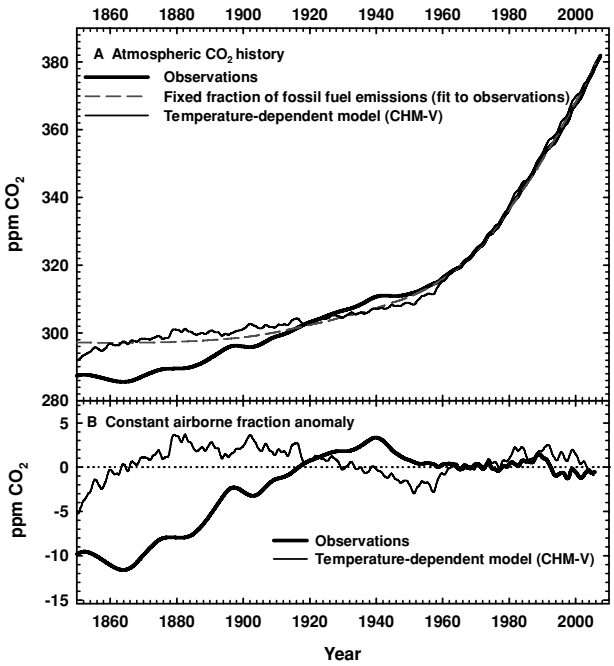

Fig. 7. (A) Atmospheric CO_2 record, atmospheric CO_2 modelled using the temperature-dependent model, and a curve depicting 57% of cumulative industrial (fossil fuel and cement) emissions. An integration constant has been added to the modelled atmospheric CO_2 to match observations from 1959 to 1979. (B) Constant airborne fraction anomaly of the atmospheric record and model results, computed by taking the difference between the atmospheric record and 57% of fossil fuel emissions.

we vary the parameters that determine the residual flux, and refit the fertilization parameter for the temperature-independent cases, or the fertilization and temperature parameters for the temperature-dependent cases, as previously. The CO_2 anomaly is again computed based on the difference between the residual flux and the fit.

For the ten temperature-independent model cases, the CO_2 anomaly curve is sensitive to assumptions, but the breaks in slope occur consistently around 1940 and 1976 (shown for six of the ten cases in Fig. 8A). The only exception is the high land use case using N fertilization (CHM-CN), where the second break moves from 1976 to 1967. When we look at the difference between the modelled CO_2 (computed using eq. 1) and 57% of fossil fuel emissions (Fig. 8B), we see that the variable ocean temperature cases (VHM-C and VLM-C) give similar results as the corresponding constant ocean temperature case (CHM-C and CLM-C). Compared with the standard case (CHM-C, shown also in Fig. 5B), the nitrogen fertilization and low land use cases are in closer agreement with the observations from 1850 to 1900, but still show too slow a rise from 1900 to 1940.

For the ten temperature-dependent cases, we consistently find improvement compared to the corresponding temperature-independent cases (Table 2). The values of Q_{10} and the fertilization parameter for all ten cases are given in Table 2. For all of the CO_2 fertilization cases where constant ocean temperature is used, the Q_{10} values are around 4–5 to within error. Allowing for ocean warming reduces the Q_{10} values to around 3. Replacing CO_2 fertilization with N fertilization yields Q_{10} values of 1.5 and 2.8. Better fits are obtained for the low land use cases than the high land use cases. The Q_{10} values for all of the cases are significantly greater than 1, which suggests that despite uncertainties, the CO_2 record contains a clear signature of warming-related releases of CO_2 to the atmosphere on multidecadal timescales. The signature emerges despite the uncertainties in the magnitude of CO_2 and N fertilization and land use.

For these temperature-dependent model cases, we find that the model accounts for 17–86% of the variance of the residual flux (using low-pass filtering of both the model and the residual flux, as above). The fraction accounted for in the high land use cases is higher (74–86%) than in the low land use cases (17–54%), with much of the variance in the former cases coming from the long-term trend, as opposed to decadal variability.

Figure 9A shows the CO_2 anomalies (as in Fig. 8A) for six of the ten temperature-dependent cases. These cases still show breaks in slope around 1940 and 1976, but the changes are less sharp than in the temperature-independent cases. These cases yield CAF anomalies (Fig. 9B) that are generally similar to the standard case (CHM-V, shown also in Fig. 7B). However, the high land use, N-fertilization case (CHM-VN) does a rather poor job of accounting for the trend from 1940 to 1960.

As an additional sensitivity test we subtract the best-fit linear trend from the temperature record, and fit ε (or γ) and Q_{10} using this new temperature record. We find that the correlation between the two fitted parameters (Q_{10} and ε or γ) is reduced from 0.70 ± 0.03 (mean and standard deviation of the cases presented in Table 2) to 0.33 ± 0.03, demonstrating that some of the correlation in the original temperature-dependent run was due to the long-term temperature trend. Using the detrended temperature record yields ε values only modestly smaller than when using the non-detrended temperature record, and estimates of Q_{10} that are still significantly larger than 1.0. Using the detrended temperature record, the quality of the fit is degraded slightly for most cases. Despite the high correlation between fitted parameters, we defend the non-detrended temperature record as being more biophysically reasonable, while acknowledging large uncertainties in parameter values.

As the specified turnover time of 2.5 yr for the small box is somewhat arbitrary, we explore additional cases where the turnover time is varied from 1 to 20 yr. This is accomplished by varying K_{a1} and K_{1a} while keeping the small box size constant (see eqs 2 and 3). We find that our ability to fit the decadal variability is not strongly dependent on the turnover time in this range. The best fits are obtained with turnover times in the range of 5–10 yr, but improvements are modest relative to the 2.5 yr case. Using time constants longer than 5 yr yields seemingly

Table 2. Best-fitting parameters, errors, and land temperature feedback for cases described in Table 1. Parameters are dimensionless unless otherwise noted

Temperature-independent model			Temperature-dependent model					
Case	ε (or γ for–CN)[1]	Error[2]	Case	ε (or γ for–VN)[1]	Q_{10}	Error[2]	γ_{AB}[3] (PgC °C^{-1})	β_{AB}[4] (PgC ppm^{-1})
CHM-C	0.67 ± 0.01	0.0565	CHM-V	0.79 ± 0.02	4.91 ± 0.93	0.0449	−25.68	2.37
CLM-C	0.18 ± 0.01	0.0391	CLM-V	0.26 ± 0.01	3.98 ± 0.66	0.0313	−15.87	0.78
CHL-C	0.85 ± 0.01	0.0556	CHL-V	0.97 ± 0.02	4.95 ± 0.91	0.0444	−28.45	2.91
CHH-C	0.50 ± 0.01	0.0560	CHH-V	0.61 ± 0.02	4.74 ± 0.92	0.0455	−22.60	1.83
CLL-C	0.36 ± 0.01	0.0396	CLL-V	0.45 ± 0.01	4.12 ± 0.67	0.0310	−18.75	1.35
CLH-C	0.01 ± 0.01	0.0386	CLH-V	0.09 ± 0.01	3.78 ± 0.65	0.0317	−13.20	0.27
VHM-C	0.75 ± 0.01	0.0594	VHM-V	0.83 ± 0.02	3.30 ± 0.67	0.0531	−20.61	2.49
VLM-C	0.25 ± 0.01	0.0463	VLM-V	0.31 ± 0.02	2.73 ± 0.52	0.0423	−12.54	0.93
CHM-CN	0.025 ± 0.001	0.0363	CHM-VN	0.027 ± 0.001	1.52 ± 0.22	0.0353		
CLM-CN	0.007 ± 0.001	0.0329	CLM-VN	0.009 ± 0.001	2.78 ± 0.39	0.0277		

[1]Units of γ are (PgC/year)$^{-1}$

[2]Error measured as the square of the difference between the model and the residual flux, divided by the number of points. Units are (ppm/yr)^2

[3]We calculate the land feedback (γ_{AB}) as defined by Friedlingstein et al. (2003). We ran our model to 2100 using a prescribed atmospheric CO_2 based on the projected IPSL (L'Institut Pierre-Simon Laplace)-uncoupled CO_2 in Friedlingstein et al. (2003) and a prescribed temperature computed using Friedlingstein et al.'s computed climate sensitivity to CO_2 ($\alpha = 0.0072$ K ppmv^{-1}). We ran this forward model with two cases: (1) using ε and Q_{10} from the temperature-dependent model, and (2) using all the same parameters except setting $Q_{10} = 1$. We then computed the difference in land carbon uptake between the cases and did a regression against temperature change to compute the feedback γ_{AB}. This approach allowed for the closest comparison to Friedlingstein et al's (2006) feedback analysis of the Coupled Climate-Carbon Cycle Model Intercomparison Project (C^4MIP) models. Further sensitivity studies showed that changes in α resulted in very little change in the feedback. Negative values of γ_{AB} denote carbon release to the atmosphere.

[4]We calculate the land flux sensitivity to CO_2 (β_{AB}), as defined by Friedlingstein et al. (2003) by taking results from the second case (see previous footnote) and regressing the cumulative land uptake against atmospheric CO_2.

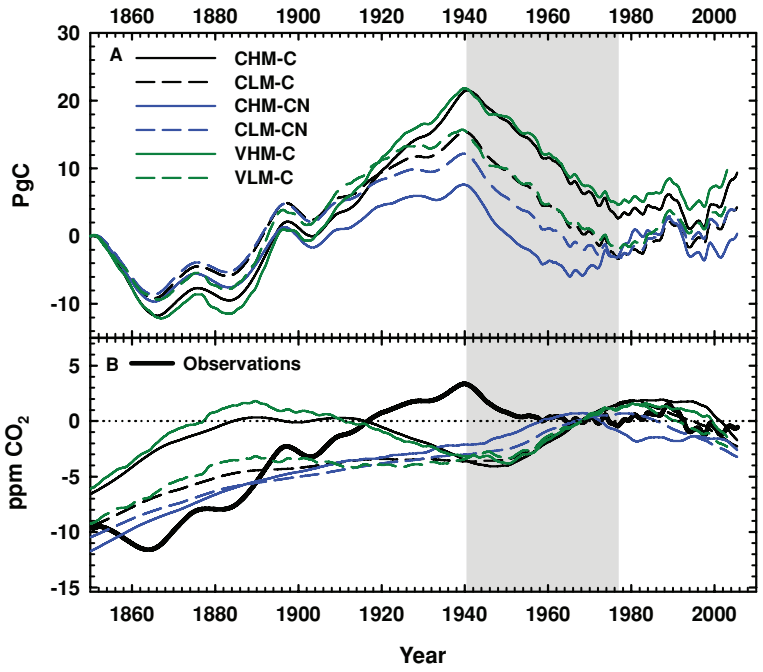

Fig. 8. (A) The integrated difference between the residual flux and temperature-independent model results for CO_2 fertilization (black and green) or N fertilization (blue). The residual flux was computed using high land use emissions (solid lines) or low land use emissions (dashed lines). For the green curves, the residual was computed using an ocean uptake that depended on SST. (B) Constant airborne fraction anomaly of the atmospheric record and temperature-independent model results, computed by taking the difference between the atmospheric record and 57% of fossil fuel emissions. See Table 1 for model definitions.

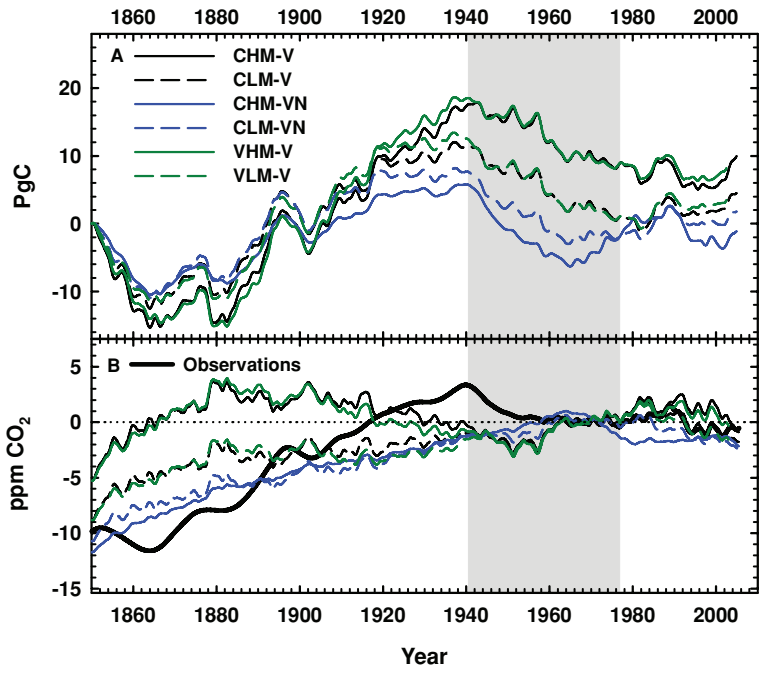

Fig. 9. (A) The integrated difference between the residual flux and temperature-dependent model results for CO_2 fertilization (black and green) or N fertilization (blue). The residual flux was computed using high land use emissions (solid lines) or low land use emissions (dashed lines). For the green curves, the residual was computed using an ocean uptake that depended on SST. (B) Constant airborne fraction anomaly of the atmospheric record and temperature-dependent model results, computed by taking the difference between the atmospheric record and 57% of fossil fuel emissions. See Table 1 for model definitions.

unrealistic values of Q_{10} (17–44 for constant ocean temperature, CO_2 fertilization cases).

We also explore four alternate temperature records to drive our land model: (1) NPP-weighted global temperature, using an NPP mask from satellite Normalized Difference Vegetation Index (NDVI) data (James and Kalluri, 1994), (2) NPP-weighted Northern extratropical temperature (north of 23.5°N), (3) NPP-weighted tropical temperature (23.5°S–23.5°N) and (4) global SST. We apply these across all temperature-dependent model cases in Table 2. We find (results not shown) that the NPP-weighted temperature records and global SST yield slightly worse fits across most cases, but the differences from the fits using the original temperature record are small. The only exceptions are: (1) the Northern extratropical temperature record yields slightly better fits for the variable ocean temperature cases and (2) the SST record yields slightly better fits for the CHL-V and CHM-VN cases.

Some studies of land box models have incorporated temperature-dependent photosynthesis (Dai and Fung, 1993; Jones et al., 2003). As an alternative, we ran our array of models using temperature-dependent photosynthesis instead of temperature-dependent respiration, replacing eq. (2) with:

$$F_{ai} = K_{ai} \times C^o_{atm} \times \left(1 + \varepsilon \Delta C_{atm}/C^o_{atm} + \gamma ff\right) \times (1 + \alpha \Delta T), \quad (4)$$

where we fit α and ε or γ, and set $Q_{10} = 1$ in eq. (3). We find that these model fits are essentially identical to fits using Q_{10}, in having fitted values of ε or γ that are unchanged, and producing similar time-dependent fluxes. Optimum values of α in these fits are –0.13 to –0.15 $(°C)^{-1}$, so the fits correspond to global average photosynthesis decreasing by 13–15% for a warming of 1°C. The similarity between these model results and results fitting Q_{10} shows that, in the context of the available constraints, we cannot distinguish the signatures of reduced photosynthesis and enhanced respiration in the records.

In the results presented above, variability on the typical El Niño timescale of 3–7 yr was removed by low-pass filtering the CO_2 record, forcing the box model to be optimized for longer timescales. Even though the model was not fit to the El Niño timescale, we find that our model can also account for much of the El Niño variability in the residual flux. Figure 10 shows the response of our standard model with the low-pass filtering removed (CHM-V, fit to match the filtered residual flux). The figure shows cases with turnover times of 2.5–10 yr for the small box, against the unfiltered residual flux. As the turnover time is increased from 2.5 to 10 yr, the amplitude of the high frequency response diminishes. These unfiltered model results account for 34–39% of the variance in the unfiltered land uptake. A similar analysis using the other temperature-dependent model cases in Table 2 (with a 2.5 yr turnover time) shows that in these cases, the model accounts for 18–46% of the variance, with the CHL-V model accounting for the highest fraction of the variance.

3.5. *Adjustment of ice core data*

As shown in Fig. 9B, some model cases (e.g. CHM-V and VHM-V) show a rise in the late 1950s that was greater by around 2 ppm than indicated by the combined ice core and direct CO_2

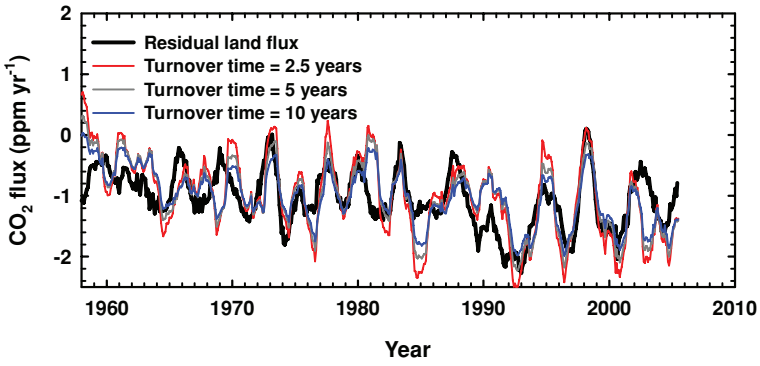

Fig. 10. Unfiltered residual land flux, showing variability on short (e.g. El Niño) timescales. Also shown are unfiltered model results from the constant SST, high land use, CO_2 fertilization run (CHM-V) using a turnover time of 2.5, 5 or 10 yr.

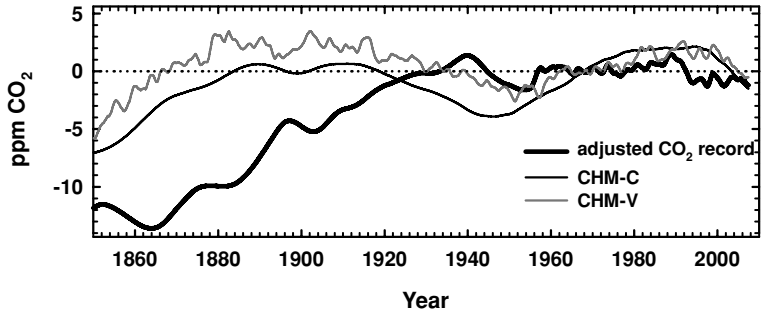

Fig. 11. Constant airborne fraction anomaly of the atmospheric record and model results, with the ice core record shifted down 2 ppm. The anomaly was computed by taking the difference between the atmospheric record and 57% of fossil fuel emissions. Models have been updated through 2007 using the fitted parameters in Table 2. Fossil fuel emissions were updated using the most recent BP data (BP, 2008). The global land air temperature record was also updated using the most recent datasets (Brohan et al., 2006). Land use emissions were extended using the extrapolations described in Section 2. See Table 1 for model definitions.

records. One possible explanation for this feature is an offset between the ice core and direct records. The ice core record has a reported uncertainty of 1.2 ppm (Etheridge et al., 1996), but this is clearly only a rough estimate and an offset in the ice core record as large as 2 ppm may be hard to firmly exclude.

To explore sensitivity to possible systematic errors in the ice core CO_2 record, we shifted the ice core record down by 2 ppm and refit our model to the adjusted data. The best-fitting parameters give lower values for both ε and Q_{10}, and higher values of γ. As shown in Fig. 11, the model now does a better job of reproducing the CO_2 record across the transition from the ice core to the direct records.

A discrepancy in 1958 might also arise due to our combining Antarctic data only (ice core record) before 1958 with the average of Antarctic (South Pole) and Mauna Loa data after 1958. However, in 1958, the difference in CO_2 concentration between Mauna Loa and the South Pole was only 0.4 ppm, which is too small to explain a 2 ppm offset.

4. Discussion

To balance the carbon budget over the past 150 yr requires a residual flux not accounted for by fossil fuel emissions, ocean uptake, or land use change. As has long been known, this residual flux has the form of a sink that grows over time with multidecadal variability. The overall growth over time can be accounted for by CO_2 or N fertilization, but these processes appear unable to account for the observed patterns of multidecadal variability. The residual flux may have a contribution from errors in the fossil fuel emissions estimates, but fossil fuel emissions are too small to contribute much uncertainty before 1958. Uncertainty in emissions more recently (e.g. 1990s) is in the range of ± 0.4 to ± 0.6 PgC yr^{-1} (Marland and Rotty, 1984). What is most critical to our analysis, however, is uncertainty in the decadal growth rate of emissions. These uncertainties are not well quantified but certainly must be much smaller than ± 0.4 to ± 0.6 PgC yr^{-1}, and therefore likely of secondary importance. A greater contribution to uncertainty in the residual flux is uncertainty in land use emissions. Although the residual flux is not well constrained due to land use uncertainty, aspects of the multidecadal variability appear to be insensitive to uncertainties.

We have shown that the multidecadal variability in the residual flux since 1940 has a connection to the variations in global climate reflected in global land air temperatures. This connection is most evident when the residual flux is expressed as an anomaly relative to the uptake accounted for by either CO_2 or N fertilization (e.g. Fig. 8A). Much of the variability in the residual land flux can be accounted for by a simple land box model

driven by global land air temperature. Although we have represented the relationship between temperature and carbon fluxes using temperature-dependent respiration or photosynthesis, the temperature dependence in our model could also be interpreted as an expression of other processes tied to temperature, such as drought or fire. Sensitivity tests of our model suggest that the carbon pools active in the multidecadal exchanges have turnover times of 2.5–10 yr. Although well resolved, the multidecadal CO_2 fluxes are typically small compared to land use and fertilization fluxes, being at most 1 PgC yr^{-1} when averaged over 10 yr.

Fluxes of carbon tied to variations in land temperature on multidecadal timescales may at least in part account for two prominent features of the CO_2 record. The plateau in CO_2 growth in the 1940s coincides with the period when temperatures stopped rising and became more constant. As shown in Figs. 7 and 9, although we can see signs of this feature in our temperature-dependent model results, the modelled plateau is offset from observations by about 2 ppm, and does not show a faster rate of increase before 1940. We have shown that when we adjust the ice core record to account for a potential 2 ppm offset, the models better reproduce the record from 1940 to 1991 (Fig. 11).

Our study also provides a context for understanding the constancy of the airborne fraction from 1958 to the present. Figures 6 and 9 demonstrate that our temperature-dependent models do a reasonable job of accounting for this constant airborne fraction. This constancy arises due to a cancellation of two effects. A reduction in the airborne fraction expected from the decrease in the growth rate of fossil fuel emissions around 1980 was compensated for by the enhanced land emissions due to a warming trend that began around the same time.

We find that the same model parameters can account for a significant fraction of the multidecadal and El Niño scale variability (Fig. 10). Zhang et al. (1997) have shown that the physical climate system (e.g. SST and sea level pressure) exhibits very similar spatial variability on decadal and interannual timescales, suggesting a close connection between the phenomenology operating on these distinct timescales. Our model results suggest that the same may be true of the carbon responses: multidecadal and interannual variability may simply be different manifestations of the same underlying phenomenology.

A link with El Niño supports our assumption that the multidecadal variability may be attributed primarily to land biosphere exchange. While the ocean and land both contribute to El Niño CO_2 variability, the land component has been shown to dominate, with the ocean component tending to oppose rather than reinforce the pattern (Keeling and Revelle, 1985; Nakazawa et al., 1997; Le Quéré et al., 2003). An extension of the oceanic component of El Niño to multidecadal timescales would presumably similarly oppose the decadal CO_2 variability. A link to land processes is also suggested by the relative success of our regressions using different temperature records, which showed that using the land temperature records yielded the best fits, while the SST record yielded inferior fits for many cases. Our interpretation, which attributes the plateau in the 1940s mostly to land processes is at odds, however, with the analysis of Trudinger et al. (2005) who attribute this feature to enhanced ocean uptake based on ice core $\delta^{13}C$ data.

Several recent studies have shown that biomass burning may be a substantial driver of the El Niño CO_2 variability (Langenfelds et al., 2002; van der Werf et al., 2004; Randerson et al., 2005). It is possible that fires could also contribute to the variations that we see on decadal timescales, but we lack records extending back to the early 20th century to test this notion.

Despite our sensitivity analysis, it remains possible that some of the multidecadal variability in CO_2 is tied to human activities. Although temperature-dependent processes on land may account for much of the anomalous CO_2 variability after 1940, it is not clear that these processes are adequate to account for anomalous fluxes before 1940. The suite of models considered here consistently underestimates the CO_2 increase from 1900 to 1940, suggesting there is a missing source of CO_2 over this period. Our results are consistent with a recent study by Ricciuto et al. (2008), which also showed difficulty reproducing the CO_2 record from 1900 to 1950 using a similar model. The difficulty could be due to errors in the land use emissions estimates in the early part of the 20th century. Decadal variability in land use emission is not well known, and could be as large as the multidecadal fluxes resolved here (McGuire et al., 2001). The land use emissions estimates of Houghton are computed based on reported land use statistics, and do not account for a range of human impacts on land that may be tied to climate, such as biomass burning. Nepstad et al. (1999) have shown that burning of downed biomass increases during El Niño-induced droughts. More work is needed to determine the importance of these influences globally and on multidecadal timescales. The difficulty in accounting for the rise from 1900 to 1940 may also result from an overestimation of land or ocean CO_2 sinks over this period. If so, this suggests that some of the processes controlling the long-term behaviour of these sinks are poorly understood.

Several studies have called attention to the possibility that recent high growth rate in CO_2 may be partly due to decreasing efficiency of CO_2 sinks (Canadell et al., 2007; Le Quéré et al., 2007). In Fig. 11, we update the records through the end of 2007 to explore the possibilities of any very recent anomalies. Fossil fuel emissions were updated using the most recent BP data (BP, 2008). The global land air temperature record was also updated using the most recent datasets (Brohan et al., 2006). Land use emissions were extended using the extrapolations described in Methods. The model was run through 2007 using the fitted parameters listed in Table 2. The largest discrepancy is seen after 1991, when the anomaly fell faster than the model predictions. This feature is almost certainly accounted for by the climate impacts of the eruption of Mt. Pinatubo, which produced large biospheric carbon fluxes via processes not adequately

represented in our model. However, the discrepancy decreases in recent years, consistent with a recovery from past perturbations. At the end of 2007, the temperature-dependent model has only a 0.5 ppm offset from the CO_2 record, showing that there are no outstanding recent discrepancies.

The relationship between the multidecadal variability of CO_2 and temperature implies a positive climate feedback. A metric for quantifying this feedback during transient warming has been developed by Friedlingstein et al. (2003, 2006), and applied across the Coupled Climate-Carbon Cycle Model Intercomparison Project (C^4MIP) models. This metric gives the change in land carbon storage in PgC per °C change in temperature. We derive this metric for our models, and find a range of −12.54 to −28.45 PgC $°C^{-1}$ (Table 2), which is on the low end of the −20 to −177 PgC $°C^{-1}$ reported for the C^4MIP models (Friedlingstein et al., 2006). Our results therefore indicate that the multidecadal variability that is resolvable in the CO_2 records is related to processes that, by themselves, do not imply a large climate feedback.

Similarly, we compute the land flux sensitivity to atmospheric CO_2 using a metric defined by Friedlingstein et al. (2003, 2006). We find a sensitivity of 0.27 to 2.91 PgC per ppm atmospheric CO_2 (Table 2). The C^4MIP models give a similar range of 0.2–2.8 PgC ppm^{-1} (Friedlingstein et al., 2006). However, most of the C^4MIP models have a sensitivity between 1.1 and 1.6 PgC ppm^{-1}, whereas for most of our cases, the sensitivity is less than 1 PgC ppm^{-1} or greater than 2 PgC ppm^{-1}, tied to the high and low land use scenarios that we employ.

An important caveat is that our analyses are only able to resolve the temperature sensitivity of the short-lived carbon pools and do not address the possibility of feedbacks tied to longer-lived carbon pools. There is no reason to discount a possible temperature sensitivity of longer-lived pools (Fang et al., 2006). Some studies suggest that long-lived pools may be at least as sensitive to temperature as short-lived pools (Knorr et al., 2005; Conant et al., 2008). However, the climate sensitivity of long-lived pools cannot be readily discerned in the global records over the past century because of confounding uncertainties in land use emissions and processes which may lead to carbon uptake on long timescales, such as CO_2 or N fertilization.

5. Conclusions

A two-box land model with a carbon flux driven by CO_2 or N fertilization and temperature-dependent respiration shows that multidecadal variations in the land CO_2 sink can be partly explained by variations in temperature, possibly through processes such as temperature-dependent respiration or fires. This response of land carbon uptake to temperature can help explain the constancy of the airborne fraction since 1980. Our analysis highlights the possibility that the ice core records might be in error by as much as 2 ppm. By allowing for a potential 2 ppm error in the ice core CO_2 record, the CO_2 plateau in the 1940s can be partly explained as well, but the record before 1940 is not well represented. Our analysis does not point to any large recent changes in the behaviour of the global carbon sinks. Furthermore, the model suggests a connection between multidecadal variability and variability on El Niño timescales, supporting the conclusion that the multidecadal variability can be attributed to carbon exchanges in the land biosphere.

The model results suggest that the multidecadal variability in the atmospheric CO_2 record can be partly accounted for by exchanges with carbon pools with relatively short turnover times in the range of 2.5–10 yr. The multidecadal responses are in the direction of positive climate feedback, i.e. warming causing additional CO_2 increase, but the exchange that we attribute to these short-lived carbon pools may be too small to constitute a significant climate feedback. The global CO_2 records appear insufficient to determine the response of carbon pools with longer turnover times because of the confounding uncertainties in land use emissions and CO_2 or N fertilization. Improving our understanding of the short-term responses, along with improved constraints on the land use and fertilization effects, will be important for resolving the signature of any long-term carbon pools in the global CO_2 record.

6. Acknowledgments

We thank Tim Barnett and three anonymous reviewers for their helpful comments. This work was supported by a grant from BP, by the National Science Foundation under Grant No. ATM-0632770, the U.S. Department of Energy under grant DE-FG02–07ER64362, and the National Aeronautics and Space Administration under grant NNG06GB98B. L. Rafelski was additionally supported by a National Science Foundation Graduate Research Fellowship.

References

Achard, F., Eva, H. D., Stibig, H.-J., Mayaux, P., Gallego, J., Richards, T. and co-authors. 2002. Determination of deforestation rates of the world's humid tropical forests. *Science* **297**, 999–1002.

Bacastow, R. and Keeling, C. D. 1973. Atmospheric carbon dioxide and radiocarbon in the natural carbon cycle: II. Changes from A.D. 1700 to 2070 as deduced from a geochemical model. In: *Carbon and the Biosphere* (eds G. M. Woodwell and E. V. Pecan). United States Atomic Energy Commission, Springfield, VA, 86–135.

Bacastow, R. and Keeling, C. 1979. Models to predict future atmospheric CO_2 concentrations. In: *Workshop on the Global Effects of Carbon Dioxide from Fossil Fuels* (eds W. P. Elliott and L. Machta). U.S. Department of Energy, Washington, DC, 72–90.

Bolin, B. 1986. How much CO_2 will remain in the atmosphere? In: *SCOPE 29: The Greenhouse Effect, Climate Change, and Ecosystems* (eds B. Bolin, B. R. Doos, J. Jager and R. A. Warrick). John Wiley & Sons, Chichester, 93–155.

BP. 2008. *BP Statistical Review of World Energy June 2008*. British Petroleum, P.L.C, London.

Brohan, P., Kennedy, J. J., Harris, I., Tett, S. F. B. and Jones, P. D. 2006. Uncertainty estimates in regional and global observed temperature changes: a new data set from 1850. *J. Geophys. Res.* **111**, D12106, doi:10.1029/2005JD006548.

Canadell, J. G., Le Quéré, C., Raupach, M. R., Field, C. B., Buitenhuis, E. T., Ciais, P. and co-authors. 2007. Contributions to accelerating atmospheric CO_2 growth from economic activity, carbon intensity, and efficiency of natural sinks. *Proc. Natl. Acad. Sci. USA* **104**, 18866–18870.

Conant, R. T., Drijber, R. A., Haddix, M. L., Parton, W. J., Paul, E. A., Plante, A. F. and co-authors. 2008. Sensitivity of organic matter decomposition to warming varies with its quality. *Global Change Biol.* **14**, 868–877.

Cox, P. M., Betts, R. A., Jones, C. D., Spall, S. A. and Totterdell, I. J. 2000. Acceleration of global warming due to carbon-cycle feedbacks in a coupled climate model. *Nature* **408**, 184–187.

Cramer, W., Bondeau, A., Woodward, F. I., Prentice, I. C., Betts, R. A., Brovkin, V. and co-authors. 2001. Global response of terrestrial ecosystem structure and function to CO_2 and climate change: results from six dynamic global vegetation models. *Global Change Biol.* **7**, 357–373.

Dai, A. and Fung, I. Y. 1993. Can climate variability contribute to the 'missing' CO_2 sink? *Global Biogeochem. Cycles* **7**, 599–609.

DeFries, R. S., Houghton, R. A., Hansen, M. C., Field, C. B., Skole, D. and Townshend, J. 2002. Carbon emissions from tropical deforestation and regrowth based on satellite observations for the 1980s and 1990s. *Proc. Natl. Acad. Sci. USA* **99**, 14256–14261.

DeLucia, E. H., Hamilton, J. G., Naidu, S. L., Thomas, R. B., Andrews, J. A., Finzi, A. and co-authors. 1999. Net primary production of a forest ecosystem with experimental CO_2 enrichment. *Science* **284**, 1177–1179.

Denman, K. L., Brasseur, G., Chidthaisong, A., Ciais, P., Cox, P. M., Dickinson, R. E. and co-authors. 2007. Couplings between changes in the climate system and biogeochemistry. In: *Climate change 2007: The physical science basis. Contribution of Working Group I to the Fourth Assessment Report of the Intergovernmental Panel on Climate Change* (eds S. Solomon, D. Qin, M. Manning, Z. Chen, M. Marquis, K. B. Averyt, co-editors). Cambridge University Press, Cambridge, United Kingdom and New York, NY, USA.

Etheridge, D. M., Steele, L. P., Langenfelds, R. L., Francey, R. J., Barnola, J.-M. and Morgan, V. I. 1996. Natural and anthropogenic changes in atmospheric CO_2 over the last 1000 years from air in Antarctic ice and firn. *J. Geophys. Res.* **101**, 4115–4128.

Fang, C., Smith, P. and Smith, J. U. 2006. Is resistant soil organic matter more sensitive to temperature than the labile organic matter? *Biogeosciences* **3**, 65–68.

Friedlingstein, P., Dufresne, J.-L., Cox, P. M. and Rayner, P. 2003. How positive is the feedback between climate change and the carbon cycle? *Tellus* **55B**, 692–700.

Friedlingstein, P., Cox, P., Betts, R., Bopp, L., von Bloh, W., Brovkin, V. and co-authors. 2006. Climate-carbon cycle feedback analysis: results from the C^4MIP model intercomparison. *J. Clim.* **19**, 3337–3353.

Galloway, J. N. and Cowling, E. B. 2002. Reactive nitrogen and the world: 200 years of change. *Ambio* **31**, 64–71.

Houghton, R. A. 1995. Effects of land-use change, surface temperature, and CO_2 concentration on terrestrial stores of carbon. In: *Biotic Feedbacks in the Global Climatic System: will the Warming Feed the Warming?* (eds G. M. Woodwell and F. T. Mackenzie). Oxford University Press, New York, 333–350.

Houghton, R. A. 2003. Revised estimates of the annual net flux of carbon to the atmosphere from changes in land use and land management 1850–2000. *Tellus* **55B**, 378–390.

Houghton, R. A. 2007. Balancing the global carbon budget. *Annu. Rev. Earth Planet. Sci.* **35**, 313–347.

House, J. I., Prentice, I. C., Ramankutty, N., Houghton, R. A. and Heimann, M. 2003. Reconciling apparent inconsistencies in estimates of terrestrial CO_2 sources and sinks. *Tellus* **55B**, 345–363.

Jain, A. K. and Yang, X. 2005. Modeling the effects of two different land cover change data sets on the carbon stocks of plants and soils in concert with CO_2 and climate change. *Global Biogeochem. Cycles* **19**, GB2015, doi:10.1029/2004GB002349.

James, M. E. and Kalluri, S. N. V. 1994. The Pathfinder AVHRR land data set: an improved coarse resolution data set for terrestrial monitoring. *Int. J. Remote Sens.* **15**, 3347–3363.

Jones, C. D., Cox, P. and Huntingford, C. 2003. Uncertainty in climate-carbon-cycle projections associated with the sensitivity of soil respiration to temperature. *Tellus* **55B**, 642–648.

Jones, C. D. and Cox, P. M. 2005. On the significance of atmospheric CO_2 growth rate anomalies in 2002–2003. *Geophys. Res. Lett.* **32**, L14816, doi:10.1029/2005GL023027.

Joos, F., Bruno, M., Fink, R., Siegenthaler, U., Stocker, T. F., Le Quéré, C. and co-authors. 1996. An efficient and accurate representation of complex oceanic and biospheric models of anthropogenic carbon uptake. *Tellus* **48B**, 397–417.

Keeling, C. D. and Revelle, R. 1985. Effects of El Niño/Southern Oscillation on the atmospheric content of carbon dioxide. *Meteoritics* **20**, 437–450.

Keeling, C. D., Bacastow, R. B., Carter, A. F., Piper, S. C., Whorf, T. P., Heimann, M. and co-authors. 1989. A three-dimensional model of atmospheric CO_2 transport based on observed winds: 1. Analysis of observational data. In: *Aspects of Climate Variability in the Pacific and the Western Americas* (ed. D. H. Peterson). American Geophysical Union, Washington, DC, 165–236.

Keeling, C. D., Whorf, T. P., Wahlen, M. and Van Der Plicht, J. 1995. Interannual extremes in the rate of rise of atmospheric carbon dioxide since 1980. *Nature* **375**, 666–670.

Knorr, W., Prentice, I. C., House, J. I. and Holland, E. A. 2005. Long-term sensitivity of soil carbon turnover to warming. *Nature* **433**, 298–301.

Langenfelds, R. L., Francey, R. J., Pak, B. C., Steele, L. P., Lloyd, J., Trudinger, C. M. and co-authors 2002. Interannual growth rate variations of atmospheric CO_2 and its $\delta^{13}C$, H_2, CH_4, and CO between 1992 and 1999 linked to biomass burning. *Global Biogeochem. Cycles* **16**, 1048, doi: 10.1029/2001GB001466.

Le Quéré, C., Aumont, O., Bopp, L., Bousquet, P., Ciais, P., Francey, R. and co-authors. 2003. Two decades of ocean CO_2 sink and variability. *Tellus* **55B**, 649–656.

Le Quéré, C., Rödenbeck, C., Buitenhuis, E. T., Conway, T. J., Langenfelds, R., Gomez, A. and co-authors. 2007. Saturation of the Southern Ocean CO_2 sink due to recent climate change. *Science* **316**, 1735–1738.

MacFarling Meure, C., Etheridge, D., Trudinger, C., Steele, P., Langenfelds, R., van Ommen, T. and co-authors. 2006. Law Dome CO_2, CH_4, and N_2O ice core records extended to 2000 years BP. *Geophys. Res. Lett.* **33**, L14810, doi:10.1029/2006GL026152.

Magnani, F., Mencuccini, M., Borghetti, M., Berbigier, P., Berninger, F., Delzon, S. and co-authors. 2007. The human footprint in the carbon cycle of temperate and boreal forests. *Nature* **447**, 848–850.

Manning, A. C. and Keeling, R. F. 2006. Global oceanic and land biotic carbon sinks from the Scripps atmospheric oxygen flask sampling network. *Tellus* **58B**, 95–116.

Marland, G. and Rotty, R. M. 1984. Carbon dioxide emissions from fossil fuels: A procedure for estimation and results for 1950–1982. *Tellus* **36B**, 232–261.

Marland, G., Boden, T. A. and Andres, R. J. 2006. Global, regional, and national CO_2 emissions. In: *Trends: A Compendium of Data on Global Change*. Carbon Dioxide Information Analysis Center, Oak Ridge National Laboratory, U. S. Department of Energy, Oak Ridge, Tenn., U.S.A.

McGuire, A. D., Sitch, S., Clein, J. S., Dargaville, R., Esser, G., Foley, J. and co-authors. 2001. Carbon balance of the terrestrial biosphere in the twentieth century: analysis of CO_2, climate and land use effects with four process-based ecosystem models. *Global Biogeochem. Cycles* **15**, 183–206.

Nakazawa, T., Morimoto, S., Aoki, S. and Tanaka, M. 1997. Temporal and spatial variations of the carbon isotopic ratio of atmospheric carbon dioxide in the western Pacific region. *J. Geophys. Res.* **102**, 1271–1285.

Nepstad, D. C., Verissimo, A., Alencar, A., Nobre, C., Lima, E., Lefebvre, P. and co-authors. 1999. Large-scale impoverishment of Amazonian forests by logging and fire. *Nature* **398**, 505–508.

Oeschger, H. and Heimann, M. 1983. Uncertainties of predictions of future atmospheric CO_2 concentrations. *J. Geophys. Res.* **88**, 1258–1262.

Pearman, G. I., Etheridge, D., de Silva, F. and Fraser, P. J. 1986. Evidence of changing concentrations of atmospheric CO_2, N_2O and CH_4 from air bubbles in Antarctic ice. *Nature* **320**, 248–250.

Plattner, G.-K., Joos, F., Stocker, T. F. and Marchal, O. 2001. Feedback mechanisms and sensitivities of ocean carbon uptake under global warming. *Tellus* **53B**, 564–592.

Randerson, J. T., van der Werf, G. R., Collatz, G. J., Giglio, L., Still, C. J., Kasibhatla, P. and co-authors. 2005. Fire emissions from C_3 and C_4 vegetation and their influence on interannual variability of atmospheric CO_2 and $\delta^{13}CO_2$. *Global Biogeochem. Cycles* **19**, GB2019, doi:10.1029/2004GB002366.

Ricciuto, D. M., Davis, K. J. and Keller, K. 2008. A Bayesian calibration of a simple carbon cycle model: The role of observations in estimating and reducing uncertainty. *Global Biogeochem. Cycles* **22**, GB2030, doi:10.1029/2006GB002908.

Sabine, C. L., Feely, R. A., Gruber, N., Key, R. M., Lee, K., Bullister, J. L. and co-authors. 2004. The oceanic sink for anthropogenic CO_2. *Science* **305**, 367–371.

Siegenthaler, U. and Oeschger, H. 1987. Biospheric CO_2 emissions during the past 200 years reconstructed by deconvolution of ice core data. *Tellus* **39B**, 140–154.

Townsend, A. R., Braswell, B. H., Holland, E. A. and Penner, J. E. 1996. Spatial and temporal patterns in terrestrial carbon storage due to deposition of fossil fuel nitrogen. *Ecol. Appl.* **6**, 806–814.

Trudinger, C., Enting, I., Etheridge, D., Francey, R. and Rayner, P. 2005. The carbon cycle over the past 1000 years inferred from the inversion of ice core data. In: *A history of Atmospheric CO_2 and its Effects on Plants, Animals, and Ecosystems* (eds J. R. Ehleringer, T. E. Cerling and M. D. Dearing). Springer, New York, 329–349.

van der Werf, G. R., Randerson, J. T., Collatz, G. J., Giglio, L., Kasibhatla, P. S., Arellano, A. F., Jr. and co-authors. 2004. Continental-scale partitioning of fire emissions during the 1997 to 2001 El Niño/La Niña period. *Science* **303**, 73–76.

Zhang, Y., Wallace, J. M. and Battisti, D. S. 1997. ENSO-like interdecadal variability: 1900–93. *J. Clim.* **10**, 1004–1020.